Advanced Steel Construction – Vol. 21 No. 4 (2025) 327–335
DOI:10.18057/IJASC.2025.21.4.5

NUMERICAL MODELLING AND DESIGN OF SQUARE CONCRETE-FILLED QN1803 STAINLESS STEEL TUBULAR STUB COLUMNS UNDER AXIAL COMPRESSION

Yao-Hui Chi [1], You-Tian Wang [2, *], Le-Tian Hai [3], Xiang Zeng [4], Bo-Wen Chen [5] and Bo-Shan Chen [4]

[1] *College of Harbour and Coastal Engineering, Jimei University, Xiamen, China*
[2] *Department of Building and Real Estate, The Hong Kong Polytechnic University, Hong Kong SAR, China*
[3] *Research Institute of Urbanization and Urban Safety, School of Civil and Resource Engineering, University of Science and Technology Beijing, Beijing, China*
[4] *School of Civil Engineering and Architecture, Hainan University, Haikou, China*
[5] *School of Civil Engineering and Architecture, Guangxi University, Nanning, China*
* *(Corresponding author: E-mail: youtian.wang@polyu.edu.hk)*

A B S T R A C T

A new generation of concrete-filled steel tubular (CFST) columns with steel tubes manufactured from QN1803 high-strength stainless steel (HSSS) was developed, which has the potential to be used extensively in demanding marine environments, and such newly developed material QN1803 offers notable advantages over traditional stainless steel including lower material cost and higher yield strength. However, no work or design rules were available for such concrete-filled QN1803 stainless steel stub columns. This study reports the results of a comprehensive numerical analysis aimed at developing new calculation formulas for concrete-filled QN1803 stainless steel square stub columns under axial compression. A nonlinear finite element (FE) model was established and validated against the existing experimental data reported by many researchers. An extensive parametric analysis comprising 460 FE models was undertaken using the validated FE models to investigate the axial loading response of CFST stub columns with QN1803 stainless steel tubes. The variables examined in the parametric analysis include the different stainless steel, wall thicknesses of the steel tube and concrete strengths. The results suggested that the ultimate bearing strength of CFST QN1803 stub columns increased by 25.3%, compared to corresponding S30408 members. The study further utilized the parametric analysis results to assess the accuracy of existing design criteria, including the Eurocode (EN 1994–1-1) (2004), American Specification (ANSI/AISC) (2022), and Australian/New Zealand standard (AS/NZS) (2017). The comparison results indicated that the existing design criteria tended to underestimate the ultimate strength of CFST stub columns with QN1803 tubes relative to the numerical results. Finally, new calculation formulas were proposed by modifying the current design standards, offering accurate and reliable predictions for these new CFST columns.

A R T I C L E   H I S T O R Y

Received: 15 December 2024
Revised: 5 June 2025
Accepted: 7 June 2025

K E Y W O R D S

Concrete-filled QN1803 stainless steel tube;
Axial compression;
Square stub columns;
Numerical analysis;
Proposed calculation formulas

1. Introduction

The concrete-filled steel tubular (CFST) columns are extensively applied in demanding marine environments, including the monopile foundations of offshore wind turbines and submerged floating tunnels [1]. In environments marked by high salinity and humidity, these structures are particularly susceptible to corrosive conditions [2-4]. Therefore, enhancing the corrosion resistance of the exterior steel tubes is essential for ensuring the structural integrity and safety [5-8]. To address this, recent innovative progress in the field of composite structures is to replace carbon steel with stainless steel (SS) as the external column tubes [9,10]. Compared to carbon steel, stainless steel offers additional benefits such as aesthetics, sustainability, recyclability, and ease of maintenance [11-13]. However, their high cost and low strength have limited their applications. Recently, the introduction of a new generation of high-strength stainless steel (HSSS), designated as QN1803, has expanded their application in the steel tubes of concrete-filled steel tubular (CFST) columns. This new material offers improved corrosion resistance in comparison with S30408 while reducing cost and providing significantly higher yield strength [14-19]. Despite these advantages, no design criteria are currently available for such CFST members with QN1803 HSSS tubes under axial loads.

Many researchers [20-22] have conducted in-depth discussions and extensive studies on the performance and design of CFST members with carbon steel tubes. Examples of such research include Uy et al. [23,24], Han et al. [25-27], Tao et al. [28], Bradford et al. [29] and Teng et al. [30]. They found that CFST members offer higher bearing capacity, improved ductility, enhanced long-term serviceability performance and greater energy absorption in comparison with traditional reinforced concrete and steel columns.

In terms of concrete-filled steel stainless steel tubular (CFSST) structures, many studies have been reported in the literature [31-36]. In 2004, Roufegarinejad et al. [37] first introduced the concept of CFST members incorporating the SS tubes. In an early investigation, Young and Ellobody [38] conducted a comprehensive series of experiments to examine how variables such as tube shape, wall thickness of tube, and strength of concrete affect the axial loading response of CFSST columns. Their research led to the formulation of revised design recommendations. Lam and Gardner [39] conducted a comprehensive investigation into the axial loading response of CFSST stub columns with circular and square cross-sections under axial loads. Their findings revealed that existing design specifications for carbon steel tend to be highly conservative. He et al. [40] performed comprehensive experimental and FE analyses on CFSST columns constructed with EN 1.4420 SS tubes, thoroughly investigating their axial loading response. Building on these findings, they updated the current design standards and introduced new design criteria. Tao et al. [41] introduced a simplified model that employs numerical methods to determine the ultimate strength of short square CFSST stub columns. In a recent investigation, Azad et al. [42-44] carried out experiments to study the impact of compression, bending, and combined loading on the structural performance of CFSST members. It was found that the existing codes cannot provide precise predictions for such CFSST columns. However, all the aforementioned research only focused on CFST members with steel tubes manufactured from traditional SS.

In parallel with these developments, recent advancements in stainless steel–concrete composite structures have introduced novel fabrication and material integration strategies. For stainless steel components, additive manufacturing (AM, also referred to as 3D printing) has emerged as a promising technique, offering improved dimensional control, material efficiency, and the ability to fabricate complex geometries without welding [45-47]. In terms of hybrid structural systems, recent research has explored several advanced forms beyond conventional CFSST columns, such as hollow double-skin stainless steel composite sections and stiffened stainless steel tubular members [33]. Among them, concrete-filled double-skin steel tubular (CFDST) sections, consisting of an inner and outer steel tube with infilled concrete, have received growing attention. CFDST columns with stainless steel outer tubes offer notable advantages over their CFSST counterparts, including enhanced strength-to-weight ratios and corrosion resistance, as well as a reduction in concrete core volume that facilitates more efficient use of materials [48].

While these studies have expanded the structural typologies of stainless steel–concrete composites, research concerning the application of newly developed high-strength QN1803 stainless steels in such systems remains limited. Recent studies [49,50] have shown that QN1803 high-strength stainless steel exhibits notable differences in material properties, including yield strength, strain hardening behavior, and ductility, compared to conventional structural steels. These differences may significantly influence the axial behavior of composite columns when QN1803 is used as the outer tube material. As a result, existing design provisions developed for mild steel composite members may not be directly applicable, and the accuracy of prevailing design codes [51-53] requires re-evaluation for such innovative CFSST systems.

This investigation presents a comprehensive numerical analysis aimed at developing new calculation formulas for concrete-filled QN1803 HSSS square stub columns under axial loads. This study seeks to build upon and extend the findings of previous research [54] by incorporating the QN1803 HSSS tubes into CFST members using numerical methods. The proposed FE modelling method was calibrated using existing test data of traditional CFSST columns. To further explore and provide design guidance for CFST stub columns under axial compression, incorporating QN1803 HSSS tubes, an extensive parametric analysis was therefore performed using the calibrated FE modelling method. The impacts of the wall thickness of the steel tubes and the infilled concrete strength on the axial loading response of such CFST members were evaluated. The parametric analysis results were compared against strength predictions provided by prevailing building standards, including the EN 1994-1-1 [51], AS/NZS 5100 [52] and ANSI/AISC 360-22 [53]. Finally, new calculation equations were subsequently recommended through modifying the existing design provisions based on the modelling results, which can provide accurate and reliable predictions for such new CFST members.

2. Summary of experimental study [44,49]

2.1. Stub column tests

A total of 21 test data were collected and summarized in this section for validating the models. Among them, nine CFSST square stub columns were tested by Dai et al. [54] previously, and the remaining 12 test data were reported by He et al. [40], Young and Ellobody [38], Lam and Gardner [39]. Dai et al. [54] performed experiments on short columns utilizing a hydraulic axial testing machine. They precisely measured axial displacements with the aid of two LVDT devices, as depicted in Fig. 1. The columns were placed under a loading condition where they were supported at the top with a pinned connection and fixed support at the bottom. It is noteworthy that the sample tubes were constructed by welding four SS plates, either austenitic or duplex, into a box-shaped section. Regarding the loading method, Young and Ellobody [38], He et al. [40], and Dai et al. [54] used displacement-controlled loading, while Lam and Gardner [39] employed load-controlled loading at 3kN/min. For a more comprehensive overview of the short column tests, refer to the study [54].

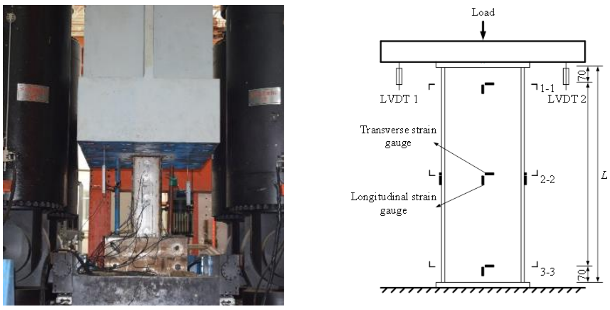

(a) Photo of experimental configuration (b) Schematic view

Fig. 1 Stub column tests reported by Dai et al. [54]

2.2. Tensile coupon tests

A total of six tensile coupons were examined by Chen et al. [49] in a previous investigation, and the mechanical properties of QN1803 HSSS was obtained. The tensile test data, summarized in Table 1, are available for conducting parameter analysis.

Table 1
Material properties [44]

Coupon ID	Thick-ness t_w/mm	Young's modulus E/GPa	0.2% proof stress $\sigma_{0.2}$/MPa	Ultimate stress σ_u/MPa
304D-T4-1	3.70	196.0	481.1	767.0
304D-T4-2	3.67	198.5	480.4	777.4
304D-T4-3	3.70	195.8	470.6	776.6
304D-T12-1	11.75	198.0	411.0	736.1
304D-T12-2	11.79	199.5	418.8	734.5
304D-T12-3	11.73	199.8	429.1	739.7

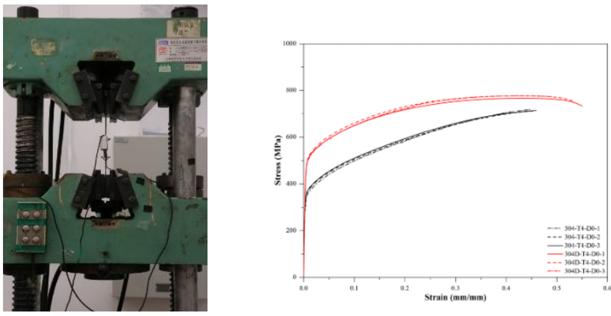

(a) Setup of tensile cotest (b) Stress-strain curves of QN1803

Fig. 2 Tensile coupon tests reported by Chen et al. [49]

A tensile test was performed using a 300 kilonewton machine, adhering to the ISO 6892-1 [55] standard. The experimental setup is presented in Fig. 2(a). Test specimens, extracted from the original, untested material, were aligned with the rolling direction of the material. For each thickness, three uniformly sized coupons were prepared. The stress-strain behavior of QN1803 is depicted in Fig. 2(b), demonstrating that its yield strength exceeds 400 MPa, confirming its classification as HSSS. The study revealed that the yield strength of QN1803 surpasses 400 MPa, marking a significant increase in comparison with S30408. A composition investigation revealed that QN1803 HSSS had a nickel content ranging from 1.5% to 2.2%, while the regularly used S30408 and S22053 have nickel contents of 8% to 11% and 4.5% to 6.5%, respectively. The above comparisons highlight that QN1803 differ significantly from S30408 in both chemical composition and material properties. The work of Chen et al. [49] illustrates comprehensive details of the experimental plan.

3. Establishment and verification of numerical models

3.1. General

To replicate the axial loading response of CFST members, a nonlinear finite element model was constructed using the ABAQUS software [56], a widely used finite element analysis software. The experimental data reported by many researchers and additional studies [38-40,54] were used for validation. Comprehensive details on the model's development and validation will be presented next.

3.2. Modelling of material properties

The stress-strain ($\sigma-\varepsilon$) behavior of SS is characterized in the numerical models using a two-stage Ramberg-Osgood equation, as expressed in Eq. (1). Previous research [42-44] has demonstrated the efficacy of this formulation in accurately representing the nonlinear response of SS in concrete-filled steel tube columns.

$$\varepsilon = \begin{cases} \frac{\sigma}{E} + 0.002\left(\frac{\sigma}{\sigma_{0.2}}\right)^n & \sigma \leq \sigma_{0.2} \\ 0.002 + \frac{\sigma_{0.2}}{E} + \frac{\sigma-\sigma_{0.2}}{E_{0.2}} + \varepsilon_u\left(\frac{\sigma-\sigma_{0.2}}{\sigma_u-\sigma_{0.2}}\right)^m & \sigma > \sigma_{0.2} \end{cases} \tag{1}$$

where ε_u is the strain corresponding to the ultimate stress σ_u, n and m are the material constants in the Ramberg–Osgood equation, representing the strain-hardening characteristics of the material.

The engineering stress (σ)-strain (ε) data were transformed into true stress (σ_{true})-strain (ε_{true}) curves using Eqs. (2) and (3). This method addresses the nonlinear responses and geometric transformations of materials under deformation, thereby enhancing the precision of the numerical models utilized in this study.

$$\sigma_{true} = \sigma(1+\varepsilon) \tag{2}$$

$$\varepsilon_{true} = ln(1+\varepsilon) - \sigma_{true}/E \tag{3}$$

The performance of concrete is simulated adopting the concrete damage plasticity model in ABAQUS [56]. This model involves defining multiple parameters, including the dilation angle, flow potential eccentricity, uniaxial-to-biaxial compressive strength ratio, tensile-to-compressive meridian stress deviator ratio, and the viscosity parameter. Based on guidelines provided in the literature [54], these values are specified as 30°, 0.1, 1.16, 0.667, and 0, respectively. The elastic modulus of the concrete (E_c) is calculated using Eq. (4) [54], and the Poisson's ratio is consistently assigned a value of 0.2.

$$E_c = 4700\sqrt{f_c'} \tag{4}$$

where f_c' is the cylinder compressive strength.

For CFSST members under compression, the confinement effect of the SS tubes induces triaxial stress states in the concrete core, resulting in mechanical behavior comparable to that of carbon steel CFST members under equivalent loading conditions. The finite element analysis employed the concrete confinement model developed by Tao et al. [41], assuming linear tensile behavior in concrete up to its tensile strength, approximated as 0.1 f_c'. Beyond this threshold, the nonlinear tensile stress-strain relationship is characterized by the fracture energy (G_F), calculated using Eq. (5).

$$G_F = (0.0469d_{max}^2 - 0.5d_{max}+26)\left(\frac{f_c'}{10}\right)^{0.7} \tag{5}$$

3.3. Finite element type and meshing

In modeling the external steel tube and concrete core, the eight-node solid element (C3D8R) from the ABAQUS element library was utilized [57-60]. This element is well-suited for simulating the behavior of both materials due to its capability to accurately capture the interaction between them, as illustrated in Fig. 3. To ensure a balance between computational accuracy and efficiency, an investigation of mesh sensitivity was conducted. Three mesh densities were examined, corresponding to global seed sizes of 1/10, 1/15, and 1/20 of the section width. The results showed that the mesh with a seed size of 1/10 of the section width slightly overestimated the ultimate axial strength (by approximately 3%), whereas the results obtained with 1/15 and 1/20 of the section width were nearly identical. Therefore, a global seed size of 1/15 of the section width was adopted for all subsequent finite element models.

3.4. Modelling of boundary and loading conditions

The interaction and boundary conditions between the tube and the core concrete were modeled using face-to-face contact. To account for potential separation after initial engagement, a hard contact approach was adopted for the normal direction. In the tangential direction, a penalty friction model was implemented to simulate sliding behavior at the steel-concrete interface. A small sliding formulation was adopted, considering the limited slippage observed under axial compression. The friction coefficient was set to 0.25, consistent with values recommended in previous studies [54]. The robustness of this assumption was confirmed by additional simulations with higher friction coefficients (0.4 and 0.6), which showed negligible influence on the axial load–displacement response. As depicted in Fig. 4, two reference points, RP1 and RP2, were created and linked to the nodes located at each end of the cross-section. For RP1, boundary conditions were set to restrict movement in all directions. Conversely, RP2 was permitted to move freely along the z-direction but was restricted in all other directions.

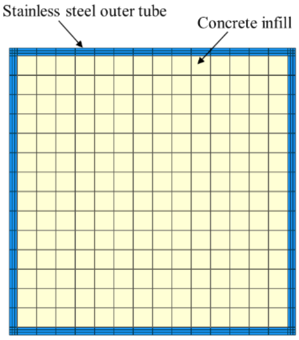

Fig. 3 Mesh configuration of FE models

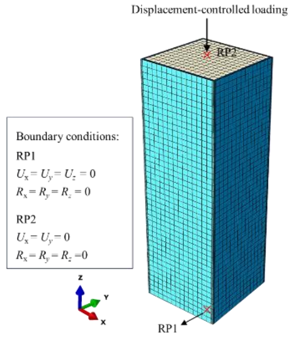

Fig. 4 Boundary conditions

3.5. Initial geometric shapes and residual stress

Initial geometric imperfections and residual stresses can significantly affect the local buckling behavior and ultimate strength of hollow steel sections. However, for concrete-filled steel tubular (CFST) stub columns, the presence of concrete core effectively restrains local out-of-plane deformations and reduces the influence of these initial imperfections. Tao et al. [41] demonstrated that this confinement not only suppresses local buckling but also plays a role analogous to that of initial geometric imperfections, thereby diminishing their influence on compressive behavior. This mitigation mechanism has also been validated in concrete-filled stainless steel tubular columns. Specifically, Han et al. [33] concluded that for short CFSST members, the effects of initial geometric imperfections and residual stresses are significantly reduced due to the stabilizing effect of the concrete infill.

Based on these findings, and considering that the QN1803 stainless steel tubes used in this study were filled with concrete and tested as stub columns, the exclusion of initial geometric imperfections and residual stresses in the finite element modeling is deemed reasonable.

Table 2
Summarized test data of CFST stub columns from literature

Source	Specimen ID	Tube material	$B \times t$ (mm)	L (mm)	f_y (MPa)	f_c' (MPa)	$N_{u,test}$ (kN)
Dai et al. [54]	A-t8C50	304	296×7.8	840	293	38.1	6290
	A-t10C50		300×9.9	840	287	38.1	7113
	A-t12C50		304×11.9	842	301	38.1	7924
	A-t8C70		296×7.8	840	293	56.6	6743
	A-t10C70		300×9.9	840	287	56.6	7947
	A-t12C70		304×11.9	840	301	56.6	8575
	A-t8C80		296×7.8	841	293	64.9	7436
	A-t10C80		300×9.9	839	287	64.9	8430
	A-t12C80		304×11.9	840	301	64.9	9257
Young and Ellobody [38]	SHS1C40	EN 1.4462	150×5.8	450	497	46.6	2768.1
	SHS1C60		150×5.8	450	497	61.9	2972.0
	SHS1C80		150×5.8	450	497	83.5	3019.9
Lam and Gardner [39]	SHS100×100×2-C30	Not provided	100×2.2	300	385	30	534
	SHS100×100×2-C60		100×2.0	300	385	53	687
	SHS100×100×2-C100		100×2.2	300	385	74	836
He et al. [40]	SHS100×100×3-C40	High-chromium grade EN 1.4420	99×3.0	299	365	49.1	830
	SHS100×100×3-C60		100×3.0	299	365	68.1	1004
	SHS100×100×3-C80		100×3.0	299	365	86.4	1162
	SHS120×120×5-C40		120×5.0	358	317	49.1	1373
	SHS120×120×5-C60		120×5.0	359	317	68.1	1566
	SHS120×120×5-C80		120×5.0	357	317	86.4	1840

3.6 Validation of numerical models

Table 2 presents a comparison of 21 laboratory test findings for CFSST members, as reported by Dai et al. [54], He et al. [40], Young and Ellobody [38], and Lam and Gardner [39]. Table 3 compares the ultimate strength estimated by numerical analysis ($N_{u,FE}$) with laboratory testing ($N_{u,test}$) [38-40,54], revealing an average $N_{u,test}/N_{u,FE}$ ratio of 0.95 with a coefficient of variation (COV) of 0.034 . Fig. 5 plots the relationship between load and axial displacement, as obtained from both laboratory testing [38-40,54] and numerical analysis. The analysis reveals that all curves exhibit strong agreement regarding ultimate strength. Nonetheless, some finite element curves display slightly greater initial stiffness in comparison with the experimental curves. This discrepancy is likely attributable to localized slipping between the loading support and the sample during testing. Fig. 6 presents the deformed configurations captured during experimental testing and finite element (FE) modeling for specimen A-t10C80. The experimental observations identified local buckling failure predominantly in the midsection of the steel tube, a phenomenon closely mirrored by the numerical simulation outcomes.

Consequently, the FE models are capable of estimating the axial loading response of CFSST members for both their ultimate strength and failure characteristics, which is supported by the negligible average difference [61-63].

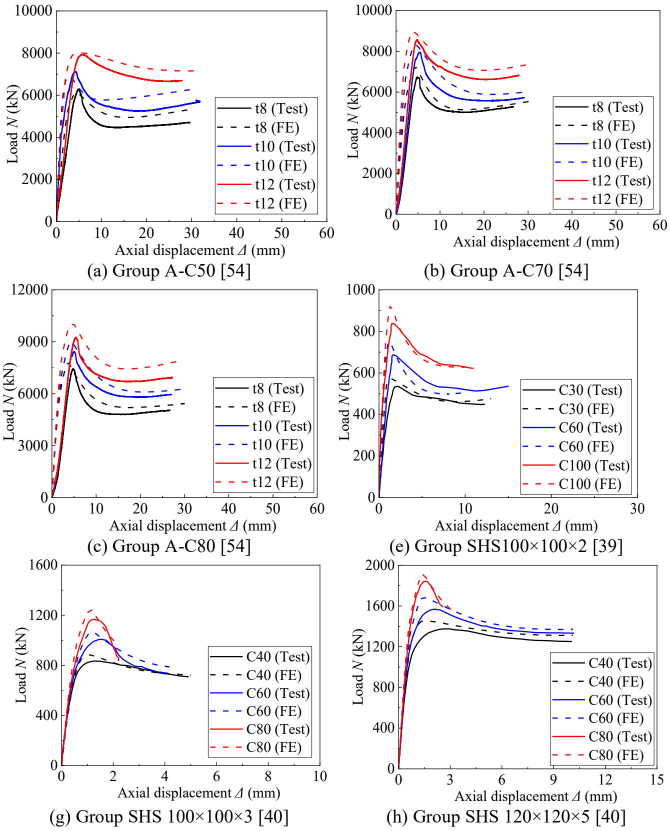

Fig. 5 Typical comparisons of test and FE load-axial displacement curves

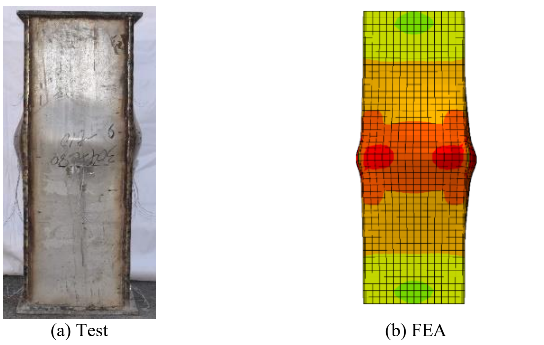

Fig. 6 Comparisons of test and FE failure modes for specimen A-t10C80 [54]

4. Parametric analysis for CFST columns with QN1803 tube

4.1. General

Following comprehensive validation of the FE model, an extensive parametric study comprising 460 models was conducted to assess the axial loading response of CFST stub column constructed with QN1803. The crucial variables examined in this investigation included the different stainless steel, wall thicknesses of the tube and concrete strengths. Table 4 details the critical parameters employed in the parametric research.

To assess how different types of stainless steel affect the load-bearing capacity of CFSST stub columns, both QN1803 and S30408 were considered as steel tubes. Noting that the mechanical properties for QN1803 and S30408 are derived from tensile tests performed by Chen et al. [49], with further details provided in Section 2.2. The steel tubes were designed to have a width (B) of 200 mm and a length (L) of 600 mm to ensure the local buckling behaviour of composite stub columns. This slenderness ratio has been widely adopted in previous CFST and CFSST studies for investigating confined local failure mechanisms [38-41]. Also, five different grades of concrete were examined in the parametric research, and the cylinder compressive strengths (f_c') were 23.7 MPa, 31.6 MPa, 39.5 MPa, 47.4 MPa, and 55.3 MPa. The constitutive laws for these concrete grades are established using the concrete damage plasticity model, as outlined in Section 3.2. The thickness (t) varies between 1 mm and 10 mm. The selected values of section width (B) and wall thickness (t) were designed to cover a broad range of width-to-thickness ratios, thereby encompassing compact, noncompact, and slender section profiles according to the classification of squarer hollow sections (SHS) in ANSI/AISC 360-22 [53]. The subsequent chapters will provide an in-depth analysis of how variations in SS types, wall thickness, and concrete strength influence the overall strength of CFSST members.

4.2. Impact of different stainless steel

Fig. 7(a) demonstrates the impact of different stainless steels on the axial behavior of CFSST stub columns. The comparison findings suggested that the CFST stub columns with QN1803 HSSS tube exhibit higher strength by 25.3% in comparison with S30408 columns. Additionally, Fig. 7(b) illustrates the load-displacement curves normalized for comparison, in which the normalized load value (N_{nor}) has been adopted in the form of $N/(\sigma_{0.2}A_s + A_c f_c')$ and the normalized displacement value ($\varDelta_{nor}$) have been taken as $\varDelta/H$. The findings reveal that both specimens can exceed a normalized load of 1.0, achieving a similar peak load of approximately 1.07. However, after reaching peak load, the specimen fabricated with QN1803 HSSS exhibits greater post-peak strength compared to S30408 columns.

4.3. Impact of tube thicknesses

Fig. 8 displays the N-$\varDelta$ and N_{nor}-$\varDelta_{nor}$ curves for typical short steel-concrete composite column with QN1803 HSSS tubes, where all columns have a consistent steel tube width of 200 mm and a concrete compressive strength of 47.4 MPa. The SS tubes come in various thicknesses, including 1 mm, 3 mm, 6 mm, 8 mm, and 10 mm. As observed from Fig. 8(a), the ultimate bearing strength of these columns significantly improves as the thickness of the steel tubes increases. The enhancement in load-bearing capacity primarily results from the increased thickness of the tubes, which enlarges the cross-sectional

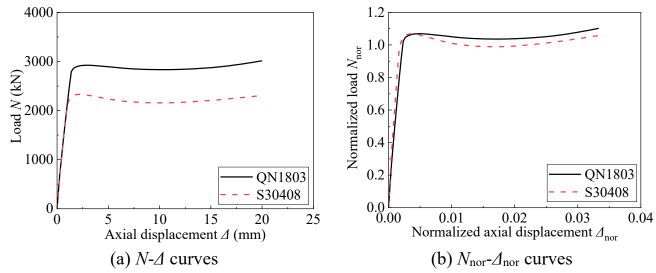

Fig. 7 Impact of stainless steel type on square CFSST stub columns

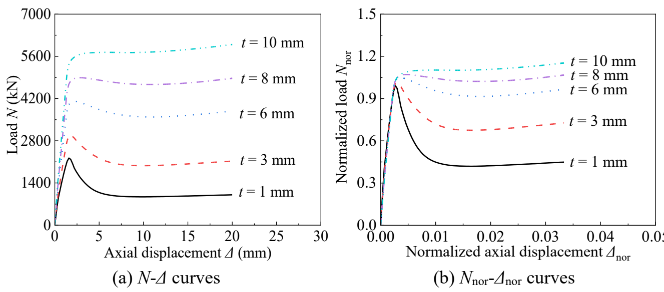

Fig. 8 Impact of outer tube thicknesses on square CFSST stub columns

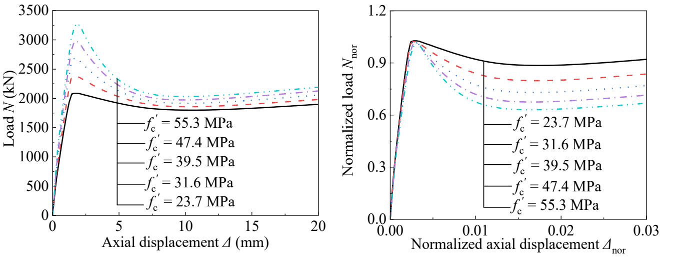

(a) N-$\varDelta$ curves (b) N_{nor}-$\varDelta_{\text{nor}}$ curves

Fig. 9 Impact of concrete strength on square CFSST stub columns

area and consequently provides more substantial confinement for the internal concrete fill. The increase in the sectional area of the tube results in a rise in the confinement factor, ξ, defined as $A_s\sigma_{0.2}/A_cf_{ck}$. A larger cross-sectional area A_s corresponds to a higher ξ value, thus strengthening the confinement imposed on the concrete. Noting that f_{ck} represents the characteristic strength of concrete, defined as $0.67f_{cu}$ in accordance with EN 1992-1-1 [64].

4.4 Impact of concrete strengths

Fig. 9 illustrates the impact of the axial loading response of the infilled concrete (f_c') on the load-bearing capacity of short steel-concrete composite columns constructed with QN1803 HSSS tubes. The analysis also compares the N-$\varDelta$ and N_{nor}-$\varDelta_{\text{nor}}$ curves. The specimens comprised steel tubes with a 200 mm diameter and 5 mm wall thickness, with concrete strengths varying from 23.7 MPa to 55.3 MPa. As seen in Fig. 9(a), the ultimate bearing capacity of these CFST stub columns increases significantly as the concrete strength rises. However, maintaining a constant thickness for the SS tube while enhancing the concrete strength reduces the level of confinement provided to the concrete core. This reduction in confinement effectiveness lowers the confinement factor ξ and, consequently, decreases the normalized load capacity at higher strain levels, as illustrated in Fig. 9(b).

5. Evaluation of current design rules

5.1. General

As previously noted, there are currently no design codes specifically addressing steel-concrete composite columns with QN1803 tubes subjected to axial loads. The existing design criteria, including Eurocode EN 1994–1-1 [51], Australian Standard AS/NZS 5100 [52] and American Specification ANSI/AISC 360-22 [53], were summarised and evaluated in this section, although they were recommended for conventional CFST members.

Table 5 summarizes the slenderness limits and material strength parameters as specified by current design codes [46-48]. Despite the slenderness limits of studied CFSST stub columns generally exceeding the limits, the objective of this investigation is to evaluate the potential for extending the applicability of these design criteria [51-53].

5.2. Evaluation of design criteria outlined in EN 1994-1-1 [51]

Eurocode EN 1994-1-1 [51] specifies a slenderness limit of $B/t \leq 52\sqrt{\frac{235}{\sigma_{0.2}}}$ for the steel tube of CFST members. Exceeding this limit necessitates the consideration of local buckling, which can be addressed using either the Effective Thickness Method (ETM) [65] or the Continuous Strength Method (CSM) [66]. Table 5 presents the adjusted local slenderness limits for the CFST cross-section $B/t \leq 52\sqrt{\frac{235}{\sigma_{0.2}}\frac{E}{210000}}$, which considered the distinct material properties of QN1803 and S30408 in comparison with carbon steel.

The axial capacity (N_{EC4}) of CFST square columns can be determined using Eq. (6). For those specimens that exceed the recommended slenderness limit, Eqs. (7) and (8) from EN 1993-1-4 [65] were employed to calculate the reduction factor (ρ_{EC}). This approach allows for the estimation of the ultimate bearing strength of CFST members featuring slender SS tubes.

$$N_{\text{EC4}} = \rho_{\text{EC}}A_s\sigma_{0.2} + A_cf_c' \tag{6}$$

$$\rho_{\text{EC}} = \frac{0.772}{\bar{\lambda}_p} - \frac{0.079}{\bar{\lambda}_p{}^2} \quad \text{but} \leq 1.0 \tag{7}$$

$$\bar{\lambda}_p = \frac{\frac{\bar{b}}{t}}{28.4\varepsilon_{\text{EC}}\sqrt{k}} \tag{8}$$

Where $\bar{b}$ is the flat element width for webs and flanges of SHS, which can be taken as B - $3t$, k is the buckling factor, which was taken as 4.

Fig. 10 contrasts the axial strength obtained from the finite element findings ($N_{\text{u,FE}}$) with the predicted strength from EN 1994-1-1 [64]. The ratio $N_{\text{u,FE}}/N_{\text{EC4}}$ is plotted against the modified slenderness ratio of the steel tube $(B/t)/\varepsilon_{\text{EC4}}$, where ε_{EC4} is defined as $\sqrt{\frac{235}{\sigma_{0.2}}\frac{E}{210000}}$. The mean values and COV of $N_{\text{u,FE}}/N_{\text{EC4}}$ for CFST stub columns with QN1803 steel tubes are 1.20 and 0.106, respectively, as presented in Table 6. Both Table 6 and Fig. 10 illustrate that the EN 1994-1-1 [51] design criteria for CFST members yield conservative predictions when applied to stubs incorporating QN1803 or S30408 steel tubes.

5.3. Evaluation of design criteria outlined in AS/NZS 5100 [52]

AS/NZS 5100 [52] utilizes a method for estimating the ultimate bearing strength of CFST members that closely resembles the approach outlined in EN 1994-1-1 [51]. The only difference is the calculation method for estimating the specified slenderness limit. The slenderness limit for the steel tube of CFST members was calculated by $b/t \leq 45\sqrt{\frac{250}{\sigma_{0.2}}\frac{E}{200000}}$, which also considers the difference in material properties of QN1803 and S30408.

The ultimate bearing strength of CFST stub column with SHS under axial loads (N_{AS}) is calculated by Eq. (9). Similarly, for those specimens that exceed the recommended slenderness limit, the reduction coefficient (ρ_{AS}) was determined using the following Eqs. (10)-(11).

$$N_{\text{AS}} = \rho_{\text{AS}}A_s\sigma_{0.2} + A_cf_c' \tag{9}$$

$$\rho_{\text{AS}} = \frac{1-\frac{0.22}{\lambda_{\text{AS}}}}{\lambda_{\text{AS}}} \quad \text{but} \leq 1.0 \tag{10}$$

$$\lambda_{\text{AS}} = \frac{\frac{1.052b}{t}}{\sqrt{k}}\sqrt{\frac{F_n}{E}} \tag{11}$$

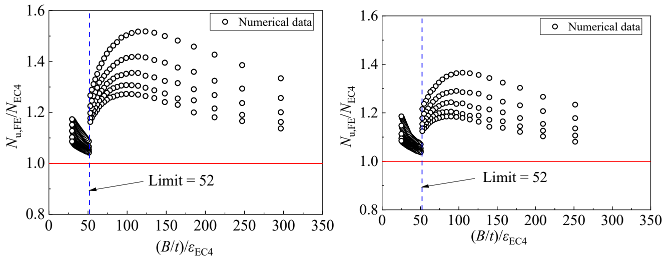

(a) QN1803 (b) S30408

Fig. 10 Evaluation of ultimate strengths obtained from parametric research with resistance predictions by EN 1994–1-1 [51]

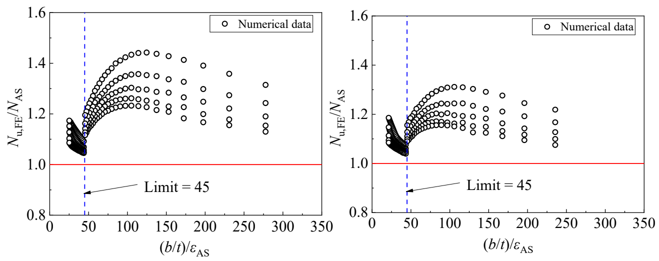

(a) QN1803 (b) S30408

Fig. 11 Evaluation of ultimate strengths obtained from parametric research with resistance predictions by AS/NZS 5100 [52]

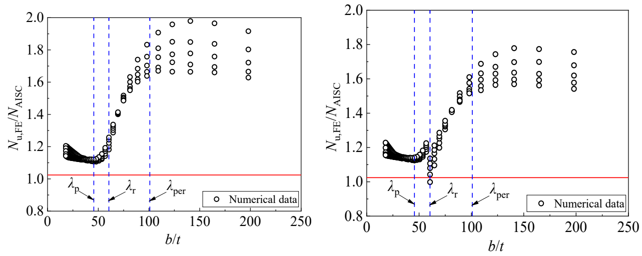

(a) QN1803 (b) S30408

Fig. 12 Evaluation of ultimate strengths obtained from parametric research with resistance predictions by ANSI/AISC 360-22 [53]

Table 3
Evaluation of the ultimate load from laboratory tests and FE studies

Source	Specimen ID	$N_{u,test}$ (kN)	$N_{u,FE}$ (kN)	$N_{u,test}/N_{u,FE}$
Dai et al. [54]	A-t8C50	6290	6084	1.03
	A-t10C50	7113	6888	1.03
	A-t12C50	7924	8016	0.99
	A-t8C70	6743	7215	0.93
	A-t10C70	7947	8320	0.96
	A-t12C70	8575	8939	0.96
	A-t8C80	7436	7774	0.96
	A-t10C80	8430	8971	0.94
	A-t12C80	9257	10000	0.93
Young and Ellobody [38]	SHS1C40	2768.1	2842	0.97
	SHS1C60	2972.0	3112	0.96
	SHS1C80	3019.9	3226	0.94
Lam and Gardner [39]	SHS100×100×2-C30	534	572	0.93
	SHS100×100×2-C60	687	752	0.91
	SHS100×100×2-C100	836	920	0.91
He et al. [40]	SHS100×100×3-C40	830	886	0.94
	SHS100×100×3-C60	1004	1066	0.94
	SHS100×100×3-C80	1162	1244	0.93
	SHS120×120×5-C40	1373	1454	0.94
	SHS120×120×5-C60	1566	1681	0.93
	SHS120×120×5-C80	1840	1910	0.96
Mean				0.95
COV				0.034

Table 4
Summary of key parameters adopted in the parametric research

Stainless steel type	D (mm)	L (mm)	t (mm)	f_c' (MPa)
QN1803, S30408	200	600	t = 1 mm to 10 mm, step 0.2 mm	23.7, 31.6, 39.5, 47.4, 55.3

Table 5
Scope of application based on cross-sectional dimensions and material strength in current design standards

Design codes	Maximum cross-sectional slenderness		f_y (MPa)	f_c' (MPa)
	Original limit	Normalized slenderness limit		
EN 1994-1-1 [51]	$\frac{B}{t} \leq 52\sqrt{\frac{235}{f_y}}$	$\frac{B}{t} \leq 52\sqrt{\frac{235}{\sigma_{0.2}}\frac{E}{210000}}$	235–460	20–50
AS/NZS 5100 [52]	$\frac{b}{t} \leq 45\sqrt{\frac{250}{f_y}}$	$\frac{b}{t} \leq 45\sqrt{\frac{250}{\sigma_{0.2}}\frac{E}{200000}}$	230–400	25–65
ANSI/AISC 360-22 [53]	$b/t \leq 5\sqrt{\frac{E}{f_y}}$	$\frac{b}{t} \leq 5\sqrt{\frac{E}{\sigma_{0.2}}}$	≤525	21–70

Table 6
Comparisons of ultimate loads obtained from parametric research with predictions from current codes

No. of data: 460		EN 1994-1-1 [51]	AS/NZS 5100 [52]	ANSI/AISC 360-22 [53]
		$N_{u,FE}/N_{EC4}$	$N_{u,FE}/N_{AS}$	$N_{u,FE}/N_{AISC}$
QN1803	Mean	1.20	1.18	1.26
	COV	0.106	0.085	0.184
S30408	Mean	1.14	1.13	1.23
	COV	0.072	0.056	0.138

Table 7
Comparisons of ultimate loads obtained from parametric research with predictions from current codes (with k =10.46)

No. of data: 460		EN 1994-1-1 [51]	AS/NZS 5100 [52]	Proposed modification based on EN 1994-1-1 [51]	Proposed modification based on AS/NZS 5100 [52]
		$N_{u,FE}/N_{EC4}^{\wedge}$	$N_{u,FE}/N_{AS}^{\wedge}$	$N_{u,FE}/N_{EC4}^{*}$	$N_{u,FE}/N_{AS}^{*}$
QN1803	Mean	1.12	1.11	1.01	1.01
	COV	0.065	0.053	0.064	0.058
S30408	Mean	1.09	1.08	1.01	1.00
	COV	0.042	0.036	0.050	0.044

Fig. 11 a comparative analysis between the ultimate load ($N_{u,FE}$) obtained from the parametric research and the ultimate load (N_{AS}) calculated by AS/NZS 5100 [52]. The ratio $N_{u,FE}/N_{AS}$ is plotted against the modified local slenderness ratio $(b/t)/\varepsilon_{AS}$. The mean values and COV of $N_{u,FE}/N_{AS}$ for CFST stub columns with QN1803 steel tubes are 1.18 and 0.085, respectively, as presented in Table 6. This indicates that the design criteria, as specified in AS/NZS 5100 [52] tend to underestimate the axial capacity of CFST members with QN1803 HSSS tubes.

5.4. Evaluation of design criteria outlined in ANSI/AISC 360-22 [53]

This study employs the design approach outlined in ANSI/AISC 360-22 [53] to assess the load-bearing capacity (N_{AISC}) of CFST short columns utilizing QN1803 and S30408 SS tubes. The ANSI/AISC 360-22 [53] design guidelines suggest categorizing concrete-filled short columns with carbon steel tubes into three classifications according to the b/t ratio of the steel tubes.

According to ANSI/AISC 360-22 [53], the cross-sectional strength (N_{AISC}) of the CFST specimens is calculated by Eq. (12). When a compact steel tube is used ((i.e. b/t falls below the limiting width-to-thickness ratio (λ_p), the tube can achieve its yield-bearing capacity ($A_s f_y$), with the concrete reaching a compressive strength of $0.85f_c'$. For non-compact steel tubes (i.e., b/t exceeds λ_p but does not exceed λ_r), the steel tube can still reach its yield-bearing capacity ($A_s f_y$), but the confinement induced on the concrete fill is diminished. In this scenario, the design utilized a compressive strength range for the confined concrete between $0.7f_c'$ and $0.85f_c'$. For slender steel tubes, where the b/t exceeds the critical value (λ_r) but remains below the maximum allowable ratio (λ_{per}), the steel tubes do not achieve their yield strength ($A_s f_y$). This results in diminished confinement for the concrete infill. Consequently, the design adopts a confined concrete compressive strength of $0.7f_c'$.

$$N_{AISC} = \begin{cases} A_s f_y + 0.85A_c f_c' & \lambda \le \lambda_p \\ P_p - \frac{P_p - P_y}{(\lambda_r - \lambda_p)^2}(\lambda - \lambda_p)^2 & \lambda_p < \lambda \le \lambda_r \\ A_s f_{cr} + 0.7A_c f_c' & \lambda_r < \lambda \le \lambda_{per} \end{cases} \tag{12}$$

In Eq. (12), the values of P_p and P_y are calculated using Eqs. (13) and (14) respectively. The critical buckling stress of the outer tube, denoted as f_{cr}, is derived using Eq. (15).

$$P_p = A_s\sigma_{0.2} + 0.85A_c f_c' \tag{13}$$

$$P_y = A_s\sigma_{0.2} + 0.7A_c f_c' \tag{14}$$

$$f_{cr} = \frac{9E_s}{\lambda^2} \tag{15}$$

Fig. 12 compares the ultimate load ($N_{u,FE}$) obtained through the parametric analysis with the corresponding NAISC values predicted using ANSI/AISC 360-22 [53]. The ratio $N_{u,FE}/N_{AISC}$ is plotted against the b/t of the steel tube. The mean values and coefficient of variation (COV) of $N_{u,FE}/N_{AISC}$ for the investigated specimens with QN1803 steel tubes are 1.26 and 0.184, respectively, as presented in Table 6. The comparison findings indicate that ANSI/AISC 360-22 [53] tends to underpredict the ultimate bearing strength of CFST members. The primary cause of this conservatism is the underestimation of the SS tube's strain-hardening effect. A similarly conservative trend is observed for stub columns with local slenderness exceeding λ_r, indicating that the slenderness limits set by ANSI/AISC 360-22 [53] may be overly restrictive, which should be evaluated carefully.

6. Proposed new calculation formulas

6.1. General

New calculation formulas were recommended by modifying the EN 1994-1-1 [51] and AS/NZS 5100 [52] in this section, and a correction factor η on the basis of k=10.67 was introduced, which considered the restraint effect of steel tubes on concrete and the strain hardening of SS. The formulas for the correction factor η were developed through regression analysis, utilizing data from 460 parametric studies. It should be noted that the buckling coefficient k given in EN 1994-1-1 [51] and AS/NZS 5100 [52] should be adjusted from 4 to 10.67 when determining the effective area of the steel tube. This adjustment is supported by a theoretical study by Bradford et al. [67], which indicated that k should be 10.67, approximately 2.67 times greater than the unfilled case, using the Rayleigh-Ritz method. This approach has also been adopted in previous studies on CFSST columns, such as Dai et al. [68,69], where k=10.67 was applied for calculating the local stability of stainless steel tubes. As presented in Figs. 13 and 14, the strength predictions (k = 10.67) calculated by EN 1994-1-1 [51] and AS/NZS 5100 [52] are compared with the parametric research findings. It could be found that the average ratios of $N_{u,FE}/N_{EC4}$ and $N_{u,FE}/N_{AS}$ are 1.12 and 1.11, respectively, indicating that the revised calculation formulas could provide more precise estimates for determining the ultimate bearing strength of CFSST members, when k is assumed to be 10.67.

The proposed correction factor η adopts a bilinear form, expressed as η = a + b $\rho\,\xi_o$, where ρ is the reduction factor accounting for local buckling and ξ_o is the confinement effect. For stainless steel tubes, the presence of strain hardening allows the steel to maintain significant post-yield strength, which may result in an actual contribution exceeding $\rho A_s f_y$, as assumed in conventional design formulations. This extended resistance not only increases the steel tube's direct axial contribution but also enhances its ability to provide continuous lateral confinement to the concrete core. Therefore, the constant term a reflects the amplified confinement effect attributed to the sustained strength of stainless steel beyond yielding, while the term b $\rho\,\xi_o$ captures the additional axial resistance arising from strain hardening and its interaction with local buckling. This formulation provides a physically informed enhancement to existing design provisions, particularly for CFST members incorporating high-strength stainless steel tubes. The detailed expressions and validation of η-based design formulas for both EN 1994-1-1 [51] and AS/NZS 5100 [52] are presented in the following sections.

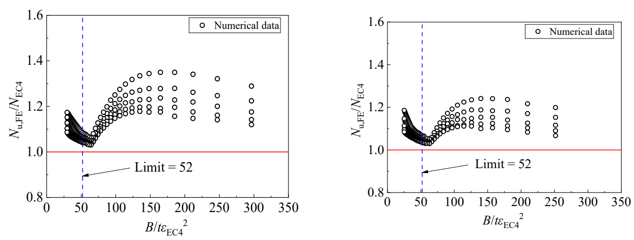

(a) QN1803 (b) S30408

Fig. 13 Evaluation of ultimate strengths obtained from parametric research with resistance predictions by EN 1994–1-1 [51] (with k = 10.67)

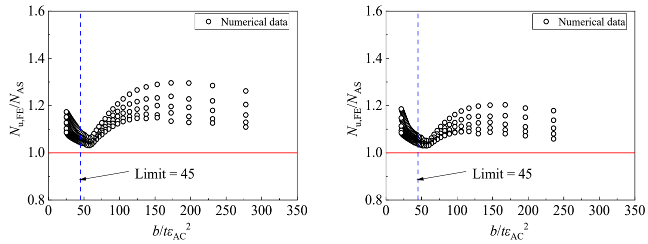

(a) QN1803 (b) S30408

Fig. 14 Evaluation of ultimate strengths obtained from parametric research with resistance predictions by AS/NZS 5100 [52] (with k = 10.67)

6.2. New calculation formulas based on modified EN 1994–1-1 [51]

In this investigation, new calculation formulas were recommended using the correction factor ηEC on the basis of modified EN 1994- [51]. The ultimate bearing strength of CFST square stub columns under axial loads (N_{EC4}^*) could be estimated by Eq. (16), and the correction factor (η_{EC}) could be calculated by Eqs. (17)-(18).

Table. 7 presents a comparison between the axial strength acquired from the parametric research and the strength predicted by modified EN 1994-1-1[51]. The mean ratios of the $N_{u,FE}$ to the predicted design strengths (N_{EC}^*) are 1.01 for both QN1803 and S30408. The associated coefficients of variation (COVs) are 0.064 for QN1803 and 0.050 for S30408. Fig.15 demonstrates that the newly recommended calculation formulas in this work offer more precise predictions for estimating the axial load-bearing capability of new CFSST members.

$$N_{EC4}{}^* = \eta_{EC} A_c f_c{}' \tag{16}$$

$$\eta_{EC} = \begin{cases} 1.12 + 1.11\rho_{EC}\xi_o & \text{for QN1803 CFST stub columns} \\ 1.04 + 1.14\rho_{EC}\xi_o & \text{for S30408 CFST stub columns} \end{cases} \tag{17}$$

$$\xi_o = \frac{A_S \sigma_{0.2}}{A_c f_c{}'} \tag{18}$$

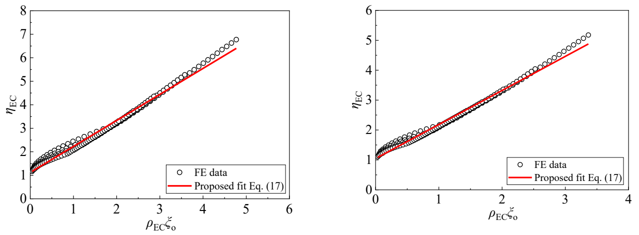

(a) QN1803 CFST stub columns (b) S30408 CFST stub columns

Fig. 15 Back calculated η_{EC} based on the ultimate load derived from parametric research varying with the $\rho_{EC}\xi_o$ and proposed algebraic characterizations

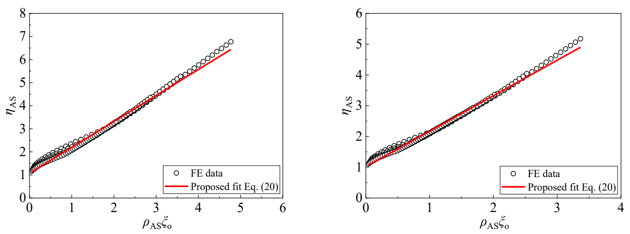

(a) QN1803 CFST stub columns (b) S30408 CFST stub columns

Fig. 16 Back calculated ηAC based on the ultimate load derived from parametric research varying with the ρACξo and proposed algebraic characterizations

6.3. New calculation formulas based on modified AS/NZS 5100 [52]

New calculation formulas were also recommended by modifying AS/NZS 5100 [52] in this investigation. Table 7 compares the axial strength from the parametric research ($N_{u,FE}$) with the strength predicted by the modified AS/NZS 5100 (N_{AS}^*), as indicated in Eqs. (19) and (20). The modified equations reveal average $N_{u,FE}/N_{AS}^*$ ratios of 1.01 and 1.00 for QN1803 and S30408, with associated coefficients of variation of 0.058 and 0.044. This demonstrates that the new calculation formulas recommended in this investigation could significantly enhance the precision of predictions for assessing the load-bearing capacity of CFSST members, as indicated in Fig. 16.

$$N_{AS}{}^* = \eta_{AS} A_c f_c{}' \tag{19}$$

$$\eta_{AS} = \begin{cases} 1.07 + 1.12\rho_{AS}\xi_o & \text{for QN1803 CFST stub columns} \\ 1.02 + 1.15\rho_{AS}\xi_o & \text{for S30408 CFST stub columns} \end{cases} \tag{20}$$

7. Conclusions

This study presents a thorough numerical analysis aimed at establishing new calculation formulas for CFST QN1803 SS square stub columns under axial loading. The key findings of this research are summarized as follows:

(1) A nonlinear finite element model was developed and validated against experimental data from various researchers. The validation process confirmed good consistency between the FE predictions and the experimental findings.

(2) Following the validation, an extensive parametric study involving 460 FE models was performed to analyze the axial loading response of CFST stub columns with QN1803 SS tubes. Key parameters investigated included variations in SS grades, steel tube wall thicknesses, and concrete strengths. The findings indicated that the ultimate bearing strength of CFST QN1803 stub columns increased by an average of 25.3% in comparison with S30408 members. Increasing the thickness of the steel tubes enhanced the ultimate bearing strength due to the larger cross-sectional area, which intensified the confinement on the internal concrete infill. Additionally, increasing the concrete strength boosted the ultimate bearing strength, although this reduced the confinement effect, leading to a drop in normalized load at higher strain levels.

(3) The ultimate bearing strength derived from the parametric research was compared to the design strength predicted by EN 1994–1-1 [51], AS/NZS 5100 [52] and ANSI/AISC 360-22 [53]. The comparison findings indicated that the existing design criteria tended to underestimate the ultimate strength of CFST stub columns with QN1803 tubes relative to the numerical results.

(4) This study recommends new calculation formulas for the compressive resistance by modifying the design equations in EN 1994-1-1 [51] and AS/NZS 5100 [53], and new parameters (η_{EC} and η_{AS}) were introduced in the new calculation methods for considering the strain hardening effects of steel tubes and the confinement effects of the SS tube on the infilled concrete. New calculation formulas recommended in this investigation demonstrated accurate and reliable predictions for the ultimate bearing strength of these new CFST members. The proposed axial strength formulations for CFSST stub columns also provide a theoretical basis for extending the design methodology to slender members or to CFST columns under combined loading conditions such as axial–bending or axial–torsional actions.

Acknowledgements

This work is supported by the Natural Science Foundation of Fujian Province, China (Grant No. 2022J01816)

References

[1] Li, G. C., Chen, B. W., Yang, Z. J., Ge, H. B., & Li, X. (2021). Axial behavior of high-strength concrete-filled high-strength square steel tubular stub columns. Adv Steel Constr, 17(2), 158-168.
[2] Wang, Y., Uy, B., Li, D., Thai, H. T., Mo, J., & Khan, M. (2023). Behaviour and design of coupled steel-concrete composite wall-frame structures. Journal of Constructional Steel Research, 208, 107984.
[3] Wang, Y., Khan, M., Uy, B., Katwal, U., Tao, Z., Thai, H. T., & Ngo, T. (2024, June). Long-term performance of steel-concrete composite wall panels under axial compression. In Structures (Vol. 64, p. 106606). Elsevier.
[4] Wang, Y., Khan, M., Li, D., Uy, B., Thai, H. T., & Ngo, T. (2023). A review on long-term behaviour of steel-concrete composite structures. Ce/papers, 6(3-4), 268-275.
[5] Feng, R., Wu, C., Chen, Z., Roy, K., Chen, B., & Lim, J. B. (2020). An experimental study on stainless steel hybrid tubular joints with square braces and circular chord. Thin-Walled Structures, 155, 106919.
[6] Feng, R., Tang, C., Roy, K., Chen, Z., Chen, B., & Lim, J. B. (2020). An experimental study on stress concentration factors of stainless steel hybrid tubular K-joints. Thin-Walled Structures, 157, 107064.
[7] Fang, Z., Roy, K., Padiyara, S., Chen, B., Raftery, G. M., & Lim, J. B. (2023, January). Web crippling design of cold-formed stainless steel channels under interior-two-flange loading condition using deep belief network. In Structures (Vol. 47, pp. 1967-1990). Elsevier.
[8] Feng, R., Tang, C., Chen, Z., Roy, K., Chen, B., & Lim, J. B. (2021). A numerical study and proposed design rules for stress concentration factors of stainless steel hybrid tubular K-joints. Engineering Structures, 233, 111916.
[9] Yan, J. B., Zhang, B., Feng, J. Y., Du, Y. S., Luo, Y. B., & Shi, Y. D. (2022). Low-temperature compression behaviour of circular stub stainless-steel tubular columns. Advanced Steel Construction, 18(3), 670-678.
[10] Fan, S. G., Ding, R. M., Han, Y. L., Chen, M. H., Liu, C. L., & Tao, Y. L. (2020). Experimental study on bearing capacity of austenitic stainless steel lipped channel columns. Advanced Steel Construction, 16(1), 65-76.
[11] Li, D., Uy, B., Aslani, F., & Hou, C. (2019). Behaviour and design of spiral-welded stainless steel tubes subjected to axial compression. Journal of Constructional Steel Research, 154, 67-83.
[12] Wang, Y., Chen, B., Wang, J., Luo, L., Li, B., Ye, Q., & Hai, L. (2025). Effect of web openings on the patch-loading resistance of QN 1803 high-strength stainless steel plate girders. Thin-Walled Structures, 113065.
[13] Wang, Y., Chen, B., Dai, P., Chen, Y., Zhang, Z., Lu, P., & Huang, C. (2025, August). Design recommendations for perforated S32001 high-strength stainless steel girders under concentrated loading. In Structures (Vol. 78, p. 109295). Elsevier.
[14] Wang, Y., Chen, B., Dai, P., Wang, Y., Song, Y., Jiang, K., & Hai, L. (2025). Experimental and numerical study on lateral-torsional buckling of welded QN1803 high-strength stainless steel I-girders. Thin-Walled Structures, 212, 113190.
[15] Chen, B., Wang, Y., Xing, Z., Lim, J. B., & Hai, L. (2024). Material properties and shear behaviour of QN1803 high-strength stainless steel plate girders. Engineering Structures, 301, 117209.
[16] Chen, B., Wang, Y., Xu, D., Yuan, H., & Yan, L. (2023). Finite element analysis and proposed design rules for 304D high-strength stainless steel I-shaped members in shear. Journal of Constructional Steel Research, 204, 107861.

[17] Chen, B., Dai, Y., Wang, Y., Wang, Y., Song, Y., Luo, L., & Hai, L. (2025). Patch-loading resistance of QN1803 and S32001 high-strength stainless steel plate girders: Experimental study and numerical simulation. Thin-Walled Structures, 206, 112681.

[18] Chen, B., Wang, Y., Wang, Y., Luo, L., Li, B., Lim, J. B., & Dai, Y. (2024). New design recommendations for QN1803 high-strength stainless-steel plate girders with web openings in shear. Journal of Constructional Steel Research, 221, 108907.

[19] Foshan Goldeco Stainless Steel Co. Ltd. Guangdong, China, 2022. https://www.goldecosteel.com/304d-stainless-steel.htm

[20] Song, Y., Li, J., & Chen, Y. (2019). Local and post-local buckling of normal/high strength steel sections with concrete infill. Thin-Walled Structures, 138, 155-169.

[21] Giakoumelis, G., & Lam, D. (2004). Axial capacity of circular concrete-filled tube columns. Journal of constructional steel research, 60(7), 1049-1068.

[22] Liew, J. R., & Xiong, D. X. (2012). Ultra-high strength concrete filled composite columns for multi-storey building construction. Advances in Structural Engineering, 15(9), 1487-1503.

[23] Uy, B. (1998). Local and post-local buckling of concrete filled steel welded box columns. Journal of constructional steel research, 47(1-2), 47-72.

[24] Uy, B. (2008). Stability and ductility of high performance steel sections with concrete infill. Journal of Constructional Steel Research, 64(7-8), 748-754.

[25] Han, L. H., Li, W., & Bjorhovde, R. (2014). Developments and advanced applications of concrete-filled steel tubular (CFST) structures: Members. Journal of constructional steel research, 100, 211-228.

[26] Han, L. H., Zhao, X. L., & Tao, Z. (2001). Tests and mechanics model for concrete-filled SHS stub columns, columns and beam-columns. Steel and Composite Structures, an International Journal, 1(1), 51-74.

[27] Han, L. H. (2002). Tests on stub columns of concrete-filled RHS sections. Journal of constructional steel research, 58(3), 353-372.

[28] Tao, Z., Song, T. Y., Uy, B., & Han, L. H. (2016). Bond behavior in concrete-filled steel tubes. Journal of Constructional Steel Research, 120, 81-93.

[29] Bradford, M. A., Loh, H. Y., & Uy, B. (2002). Slenderness limits for filled circular steel tubes. Journal of Constructional Steel Research, 58(2), 243-252.

[30] Teng, J. G., Wang, J. J., Lin, G., Zhang, J., & Feng, P. (2021). Compressive behavior of concrete-filled steel tubular columns with internal high-strength steel spiral confinement. Advances in Structural Engineering, 24(8), 1687-1708.

[31] Lam, D., Yang, J., & Dai, X. (2019, October). Finite element analysis of concrete filled lean duplex stainless steel columns. In Structures (Vol. 21, pp. 150-155). Elsevier.

[32] Dai, P., Yang, L., Wang, J., & Zhou, Y. (2020). Compressive strength of concrete-filled stainless steel tube stub columns. Engineering Structures, 205, 110106.

[33] Han, L. H., Xu, C. Y., & Tao, Z. (2019). Performance of concrete filled stainless steel tubular (CFSST) columns and joints: Summary of recent research. Journal of Constructional Steel Research, 152, 117-131.

[34] Uy, B., Tao, Z., & Han, L. H. (2011). Behaviour of short and slender concrete-filled stainless steel tubular columns. Journal of Constructional Steel Research, 67(3), 360-378.

[35] Ellobody, E. (2007). Nonlinear behavior of concrete-filled stainless steel stiffened slender tube columns. Thin-Walled Structures, 45(3), 259-273.

[36] Hassanein, M. F. (2010). Numerical modelling of concrete-filled lean duplex slender stainless steel tubular stub columns. Journal of constructional steel research, 66(8-9), 1057-1068.

[37] Roufegarinejad, A., Uy, B., Bradford, M. A., Deeks, A. J., & Hao, H. (2005). Behaviour and design of concrete filled steel columns utilising stainless steel cross sections under combined actions. In Developments in Mechanics of Structures and Materials: Proceedings of the 18th Australasian Conference on the Mechanics of Structures and Materials, Perth, Australia, 1-3 December 2004.

[38] Young, B., & Ellobody, E. (2006). Experimental investigation of concrete-filled cold-formed high strength stainless steel tube columns. Journal of Constructional Steel Research, 62(5), 484-492.

[39] Lam, D., & Gardner, L. (2008). Structural design of stainless steel concrete filled columns. Journal of Constructional Steel Research, 64(11), 1275-1282.

[40] He, A., Wang, F., & Zhao, O. (2019). Experimental and numerical studies of concrete-filled high-chromium stainless steel tube (CFHSST) stub columns. Thin-Walled Structures, 144, 106273.

[41] Tao, Z., Uy, B., Liao, F. Y., & Han, L. H. (2011). Nonlinear analysis of concrete-filled square stainless steel stub columns under axial compression. Journal of Constructional Steel Research, 67(11), 1719-1732.

[42] Azad, S. K., Li, D., & Uy, B. (2020). Axial slenderness limits for duplex and lean duplex stainless steel-concrete composite columns. Journal of Constructional Steel Research, 172, 106175.

[43] Azad, S. K., Li, D., & Uy, B. (2020). Axial slenderness limits for austenitic stainless steel-concrete composite columns. Journal of Constructional Steel Research, 166, 105856.

[44] Azad, S. K., Li, D., & Uy, B. (2021). Compact and slender box concrete-filled stainless steel tubes under compression, bending, and combined loading. Journal of Constructional Steel Research, 184, 106813.

[45] Buchanan, C., & Gardner, L. (2019). Metal 3D printing in construction: A review of methods, research, applications, opportunities and challenges. Engineering Structures, 180, 332-348.

[46] Huang, Y., Yang, L., Liu, M., & Xu, K. (2025). Numerical study and design of WAAM stainless steel SHS stub columns under axial compression. Journal of Constructional Steel Research, 227, 109419.

[47] Huang, Y., Yang, L., & Xin, Q. (2023). Novel geometrical model and design mechanical parameters for CMT-WAAM stainless steel. Journal of Constructional Steel Research, 210, 108071.

[48] Ban, H., Zeng, Z., Zhang, L., Wang, F., Yun, X., & Dai, P. (2025). Numerical analysis and design of concrete-filled double skin CHS with 316L+ Q355 stainless-clad bimetallic steel outer tubes under axial compression. Engineering Structures, 329, 119796.

[49] Chen, B., Wang, Y., Xing, Z., Lim, J. B., & Hai, L. (2024). Material properties and shear behaviour of QN1803 high-strength stainless steel plate girders. Engineering Structures, 301, 117209.

[50] Chen, B., Wang, Y., Xu, D., Yuan, H., & Yan, L. (2023). Finite element analysis and proposed design rules for 304D high-strength stainless steel I-shaped members in shear. Journal of Constructional Steel Research, 204, 107861.

[51] EN 1994–1-1:2004. Eurocode 4: Design of composite steel and concrete structures - Part 1-1: General rules and rules for building. European Committee for Standardization, Brussels;2004.

[52] AS/NZS 5100.6:2017. Bridge design, Part 6: steel and composite construction, Australian/New Zealand Standards, Sydney, Australia; 2017.

[53] ANSI/AISC 360-22. Specification for structural steel buildings. American Institute of Steel Construction (AISC), Chicago;2022.

[54] Dai, P., Yang, L., Wang, J., Ning, K., & Gang, Y. (2022). Compressive behavior of concrete-filled square stainless steel tube stub columns. Steel and Composite Structures, 42(1), 91-106.

[55] ISO 6892-1: 2009. Metallic Materials − Tensile Testing − Part 1: Method of Test at Room Temperature. International Organization for Standardization, Geneva, Switzerland, 2009.

[56] ABAQUS. Analysis user's manuals and example problems manuals, version 2021 Providence, Rhode Island: Abaqus Inc.; 2021.

[57] Wang, Y., Khan, M., Uy, B., Lim, L., Thai, H. T., & Ngo, T. (2025). Behaviour, design and performance of steel-concrete composite walls in fire. Journal of Constructional Steel Research, 227, 109408.

[58] Mo, J., Uy, B., Li, D., Thai, H. T., & Wang, Y. (2022). Behaviour and design of composite walls under axial compression. Journal of Constructional Steel Research, 199, 107635.

[59] Mo, J., Uy, B., Li, D., Thai, H. T., & Wang, Y. (2023). Behaviour and design of composite walls under lateral loading and combined loading. Journal of Constructional Steel Research, 210, 108087.

[60] Li, D., Uy, B., Mo, J., Wang, Y., & Thai, H. T. (2023). Behaviour and design of steel and composite beam connections to composite walls. Journal of Constructional Steel Research, 206, 107915.

[61] Zhu, L., Jiang, Y., Liu, Z., Wang, Y., Wang, W., & Chen, B. (2024, July). Web crippling behaviour of high-strength aluminium alloy channel-shaped members with strengthened web holes: Numerical study and new design rules. In Structures (Vol. 65, p. 106690). Elsevier.

[62] Tahmasebinia, F., Wang, Y., Wu, S., Ho, J., Shen, W., Ma, H., ... & Marroquin, F. A. (2021). Advanced structural analysis of innovative steel–glass structures with respect to the architectural design. Buildings, 11(5), 208.

[63] Gao, L., Wang, Y., Wang, J., Yuan, J., Chen, B., & Bai, L. (2025). Experimental and numerical investigation on global-stability of welded BS700 high-strength steel beams. Journal of Constructional Steel Research, 227, 109373.

[64] EN 1992-1-1, Eurocode 2, Design of Concrete Structures – Part 1-1: General Rules and Rules for Buildings, CEN, Brussels, 2004.

[65] EN 1993-1-4: 2006+A1: 2015. Eurocode 3: Design of Steel Structures - Part 1–4: General Rules- Supplementary Rules for Stainless Steels. European Committee for Standardization (CEN), Brussels;2015.

[66] Gardner, L., Yun, X., & Walport, F. (2023). The continuous strength method–review and outlook. Engineering Structures, 275, 114924.

[67] Bradford, M. A., Wright, H. D., & Uy, B. (1998). Local buckling of the steel skin in lightweight composites induced by creep and shrinkage. Advances in Structural Engineering, 2(1), 25-34.

[68] Dai, P., Yang, L., Yun, X., Wang, F., & Zhang, L. (2024). Experimental study of concrete-filled stainless steel tubular stub columns with circular and square cross-sections subjected to combined compression and bending. Engineering Structures, 305, 117773.

[69] Dai, P., Yang, L., Zhang, L., & Ban, H. (2025, August). Structural behaviour and design of concrete-filled stainless steel tubular stub columns with circular and square cross-sections subjected to combined compression and bending. In Structures (Vol. 78, p. 109162). Elsevier.